Electron hole pair mediated vibrational excitation in CO scattering from Au(111): Incidence energy and surface temperature dependence

Authors

Pranav R. Shirhatti[a,b], Jörn Werdecker[a,b,c], Kai Golibrzuch[a,b], Alec M. Wodtke[a,b], Christof Bartels[a,b, 1)]

[a] Institute for Physical Chemistry, Georg August University of Göttingen, 37077 Göttingen, Germany

[b] Max Planck Institute for Biophysical Chemistry, 37077 Göttingen, Germany

[c] Present address: Laboratoire de Chimie Physique Moléculaire, Ecole Polytechnique Fédérale de Lausanne, 1015 Lausanne, Switzerland

Abstract

We investigated the translational incidence energy (E_i) and surface temperature (T_s) dependence of CO vibrational excitation upon scattering from a clean Au(111) surface. We report absolute $v = 0 \rightarrow 1$ excitation probabilities for E_i between 0.16 and 0.84 eV and T_s between 473 and 973 K. This is now only the second collision system where such comprehensive measurements are available – the first is NO on Au(111). For CO on Au(111), vibrational excitation occurs via direct inelastic scattering through electron hole-pair mediated energy transfer – it is enhanced by incidence translation and the electronically non-adiabatic coupling is only about 2 to 3 times weaker than in NO scattering from Au(111). Vibrational excitation via trapping desorption channel dominates at E_i = 0.16 eV and quickly disappears at higher E_i.

1) Author to whom correspondence should be addressed.
Email: cbartel@gwdg.de

Introduction

Studying vibrational energy transfer between small molecules and well defined surfaces provides insights into mechanisms of energy flow relevant to adsorbate surface chemistry [1-3]. For example, Kay and coworkers [4] have shown that the vibrational excitation probability of NH_3 (umbrella mode) scattered from a Au(111) surface increases monotonically with the translational incidence energy (E_i) above a threshold energy close to the vibrational excitation. The surface temperature (T_s) had no influence on the vibrational excitation probability. Here, vibrational excitation occurs via direct coupling to the translational incidence energy in an electronically adiabatic manner. On the other hand, NO scattering from Ag(111) [5] and Au(111) [6, 7] surfaces showed vibrational excitation that is strongly enhanced by surface temperature, following a pseudo-Arrhenius law where the effective activation energy is the vibrational excitation energy. While the translational incidence energy of NO molecules also enhanced vibrational excitation, no threshold was observed. In this case, the vibrational excitation occurs via coupling of the molecular vibration to the hot electron hole pairs of the metal (EHP-V).

The EHP-V energy transfer observed for NO/Ag(111) and NO/Au(111) is an example of the breakdown of the Born-Oppenheimer approximation (BOA).[8] The availability of detailed experimental data especially for NO/Au(111) [6, 9, 10], has triggered the development of several theoretical approaches that go beyond the BOA, explicitly describing the coupling of nuclear and electronic degrees of freedom.[2, 11-14] Extending the study of EHP-V energy transfer to other systems addresses questions of generality and validity for post-Born-Oppenheimer theories.

In this paper, we report comprehensive measurements of absolute vibrational excitation probabilities for the recently reported EHP-V energy transfer for CO collisions with Au(111).[15] This system behaves similarly to NO on Ag/Au, but it is complicated by the presence of trapping/desorption, which is important at low E_i.[16] Making use of absolute vibrational excitation probabilities, we characterize the two channels contributing to vibrational excitation of CO on Au(111).

Methods

Some essential features of the experimental set-up are provided in the following section. For a more detailed description the reader is referred to Ref.[17] A schematic diagram of the experimental set-up is shown in Fig. 1.

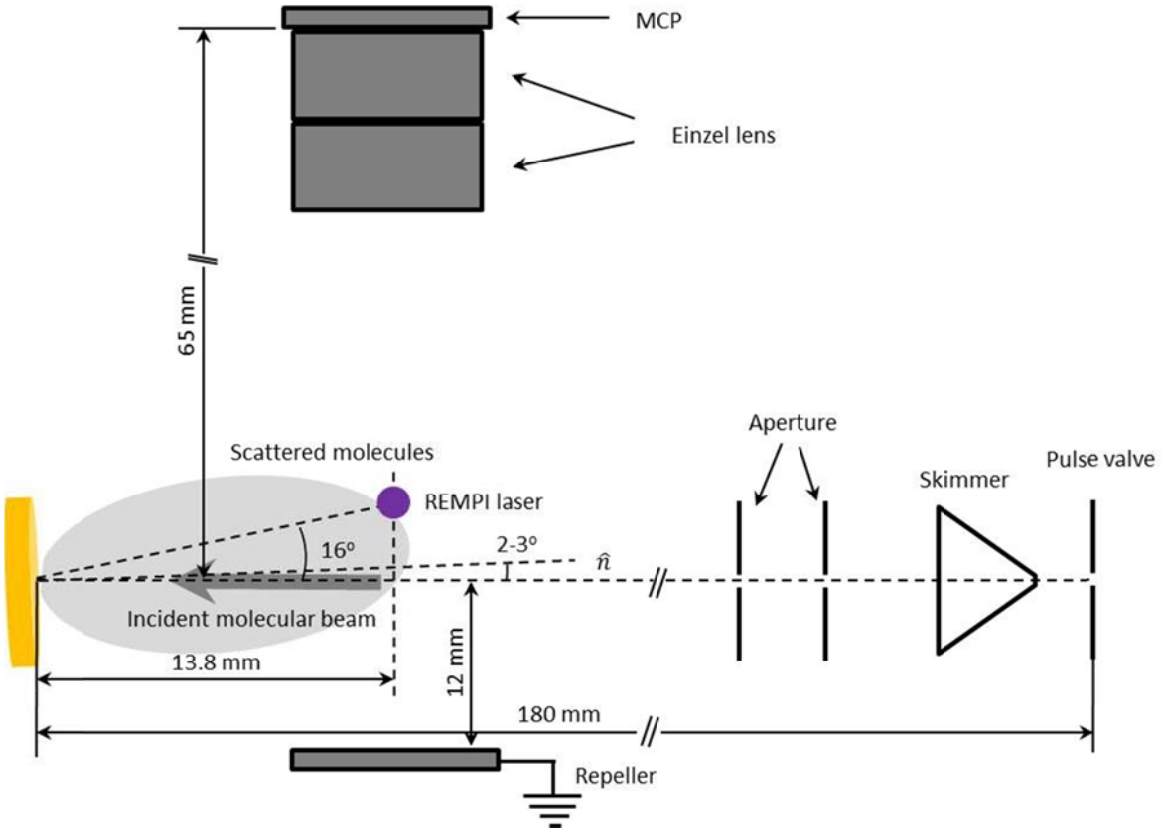

Figure 1: A schematic diagram of the experimental set up. A supersonic expansion of the CO molecules with suitable carrier gas is produced by the pulse valve. This expansion is made to pass through a skimmer and two apertures downstream to obtain a collimated molecular beam before it collides with the Au(111) surface. The surface was tilted upwards (2-3 degrees) in these experiments. The scattered molecules were detected at a position vertically offset from the incident beam (~ 10 degrees from the specular angle) in order to minimize the background caused by the non-resonant ionization of the incident beam.

The apparatus consists of four interconnected chambers: (1) source chamber, (2) differential pumping-1 stage, (3) differential pumping-2 stage and (4) UHV surface science chamber. In the source chamber, a supersonic jet expansion of the CO molecules with a suitable carrier gas (H_2/Ne) was produced using a home-built, piezo-electrically driven pulsed nozzle (stagnation pressure: 3 bar, temperature: 300 K, nozzle diameter: 1 mm). The expanding gas passes through a skimmer (1.5 mm opening diameter, Beam Dynamics) and subsequently through two circular apertures of 3 mm and 2 mm diameters, respectively, before it enters the UHV chamber as a collimated molecular beam. The typical duration (FWHM) of the molecular beam is 100-150 microseconds when it collides with the Au(111) surface, which is placed ~180 mm away from the pulsed valve opening. Typically, the pressure in the UHV chamber was 2×10^{-10} Torr and 2×10^{-9} Torr (unscaled ion gauge readings) with the molecular beam off and on, respectively. The mean E_i of the CO molecules was varied in the range of 0.16 to 0.84 eV by using different mixing ratios and carrier gases (Table 1). The fraction of

the molecules in the $v = 1$ state in the incident molecular beam was measured to be less than 10^{-4}.

Table 1: Characteristics of the molecular beams used in the experiments. ⟨E⟩ denotes the mean value and ΔE/⟨E⟩ denotes the width of the energy distribution, where $\Delta E = \sqrt{\int (\langle E \rangle - E)^2 \, dE}$. The typical fraction of the molecules in the $v = 1$ state in the incoming beam was < 0.01%.

Gas mixture composition	⟨E⟩(eV)	ΔE/⟨E⟩ (%)
2% CO + 98% H_2	0.84	8.6
5% CO + 95% H_2	0.65	8.4
10% CO + 90%H_2	0.50	8.7
15% CO + 85%H_2	0.42	9.4
20%CO + 80% H_2	0.34	8.8
4 % CO + 36% H_2 + 60% Ne	0.16	7.0

The Au(111) single crystal (orientation accuracy ~1°, purity 99.999%, MaTeck GmbH) is housed in the UHV chamber, mounted on a sample holder with tungsten wires. The crystal can be conductively heated by resistively heating the tungsten wires. The temperature is monitored by a K-type thermocouple attached on the edge of the crystal. Prior to each set of measurements for a given incidence energy, the surface was cleaned by sputtering with 3 keV Argon ions for 20-25 min. Subsequently, the crystal was annealed at 970-1000 K for 30-40 minutes to recover the (111) surface. The surface cleanliness was checked using Auger electron spectroscopy.

The molecular beam was incident on the surface at 2-3 degrees away from normal incidence and the scattered molecules were detected at a position vertically offset from the incident beam (~10 degrees from the specular reflection angle, see Fig. 1). This offset along the vertical axis minimizes background signal arising from the non-resonant ionization of the incident molecular beam. The CO molecules in the $v = 0$ and $v = 1$ state (ground electronic state) were detected using a 2+1 Resonantly Enhanced Multiphoton Ionization (REMPI) scheme via the $B^1\Sigma^+$ state. The resulting ions were extracted using a combination of two electrostatic lenses and a grounded repeller plate. These ions were detected using a dual micro channel plate (MCP) detector, with the plates arranged in a Chevron configuration.

Calculation of the absolute vibrational excitation probability

The approach used for the calculating the absolute vibrational excitation probability is similar to that used earlier for NO scattering from Au (111) and CO scattering from Au(111).[7, 15] The key features of this method are outlined briefly below.

The vibrational excitation probability in this work is defined by the following equation:

$$P(v = 0 \rightarrow i) = \frac{N_i}{\Sigma N_i}$$

Where N_i is the population in the i^{th} vibrational state in the scattered beam. In the present case of CO ($v = 0$) scattering from a Au(111) surface, for the temperature range studied (473-973 K), the molecules largely scatter back in $v = 0$ and a small fraction (< 1%) of the molecules scatter back in $v = 1$. The population in the higher vibrational states is negligibly small. Thereby, the above equation can be reduced to the following:

$$P(v = 0 \rightarrow 1) \cong \frac{N_1}{N_0 + N_1}$$

The practical implementation of this scheme requires the measurement of N_i (or a quantity proportional to it) for i = 0 and 1. It should be noted that the population of the scattered molecules in the $v = 0$ and 1 states are distributed over a large number of rotational states. Additionally, the scattered molecules also arrive with a temporal and angular distribution that, in general, can depend on the final vibrational state. Hence, it is necessary to account for these effects in the evaluation of the vibrational excitation probabilities. The measured signals also have to be scaled to account for differences in experimental parameters such as the laser power and the MCP gain. This enables us to make a meaningful comparison among the different datasets.

The scattering rotational state distributions in $v = 0$ and 1 were obtained by measuring the 2+1 REMPI spectra via the $B^1\Sigma^+$ state using the Q(0,0) and Q(1,1) bands, respectively. Since the Q(1,1) branch lines overlaps the O(0,0) lines, the observed spectra were fit to a sum of O(0,0) and Q(1,1) lines and the Q(1,1) component was extracted. In these measurements, the REMPI laser was set at a fixed delay with respect to the nozzle opening time. These measurements were carried out at 11 different surface temperatures ranging from 473 to 973 K in steps of 50 K.

The arrival time distributions of the scattered molecules in $v = 0$ and 1 (at different surface temperatures) were measured by scanning the REMPI laser in time with respect to the incoming pulsed beam. The angular distributions of the scattered molecules were measured by moving the REMPI beam along a plane perpendicular to the incident beam, covering scattering angles from approximately –40 to 40 degrees from the surface normal. For detection of $v = 0$, the REMPI

wavelength was chosen such that the high J states (populated only in the scattered beam) were detected.

Estimation of uncertainties

The major uncertainty in the measurements arises from fluctuations in the laser power, which were measured to be about 5%. In addition, error is introduced due to variations in MCP gain caused by the variation in the MCP voltage, which was measured to be of the order of ~0.5%. Uncertainties in the fitting parameters were also taken into account. The individual errors were propagated using Gaussian error propagation (assuming that the errors are independent and random) to estimate the uncertainties in the derived vibrational excitation probabilities. The reported error bars are 95% confidence intervals.

Results and discussion

Some examples of the REMPI spectra of the scattered CO molecules in the Q(1,1) band region measured at different surface temperatures and translational incidence energies are shown in Fig. 2. Clearly, the intensity of the Q(1,1) band increases with increasing surface temperature.

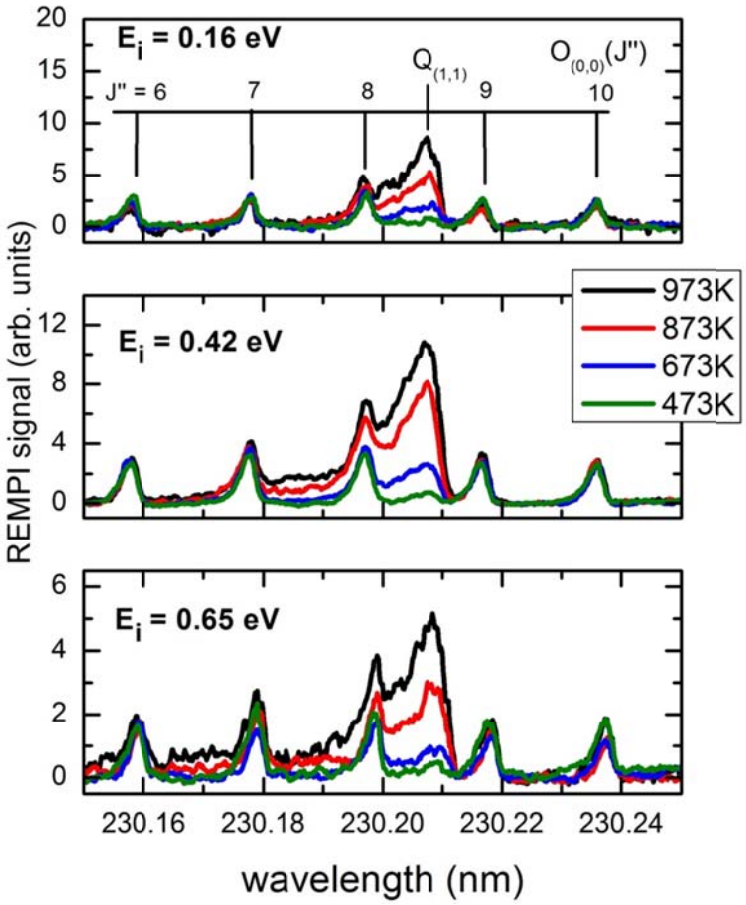

Figure 2: Examples of REMPI spectra of the scattered CO ($v = 1$)molecules measured via the Q(1,1) band at different surface temperature for three different E_i. Clearly, for a given E_i it can be seen that the intensity of the Q(1,1) band increases with T_s, whereas the intensity of the nearby O(0,0) branch lines does not.

In order to quantify the change in the CO $v = 1$ population in the scattered flux as a function of T_s, the integrated intensity of the Q(1,1) band has to be evaluated. Since the Q(1,1) band is overlapped with the nearby O(0,0) branch lines, we fitted the observed REMPI spectra to a sum of the Q(1,1) and the O(0,0) spectra using the intensity of each band as a fit parameter. The best fit parameters were used to evaluate the Q(1,1) spectrum and its integrated value. The Q(0,0) band was integrated directly (numerically) as the overlapping S(0,0) band has negligible intensity (relative to the Q(0,0) band).[18]

Both the $v = 0$ and 1 rotational distributions show deviations from a thermal distribution and depend strongly on E_i, consistent with direct inelastic scattering (see Fig. 3).[19] Hence, Q(1,1) and Q(0,0) bands were fit using an empirical non-thermal rotational state distribution of the following form:

$$N(J) = F_{\mathrm{th}}(J, T_{rot}) + a_r \times Exp[-((J - a_0)/a_1)^2]$$

Where F_{th} is a Boltzmann distribution and the second term represents a non-thermal component produced by a rotational rainbow. The non-thermal component is modelled as a Gaussian function with the parameters a_r, a_0 and a_1 representing its amplitude, center and width, respectively. The quantities a_r, a_0 and a_1 and T_{rot} were obtained from fitting the observed spectra. Few examples of the fit are shown in Fig 3 (lower panel). Additional fits and the best fit parameters obtained are provided in the supplementary information[20].

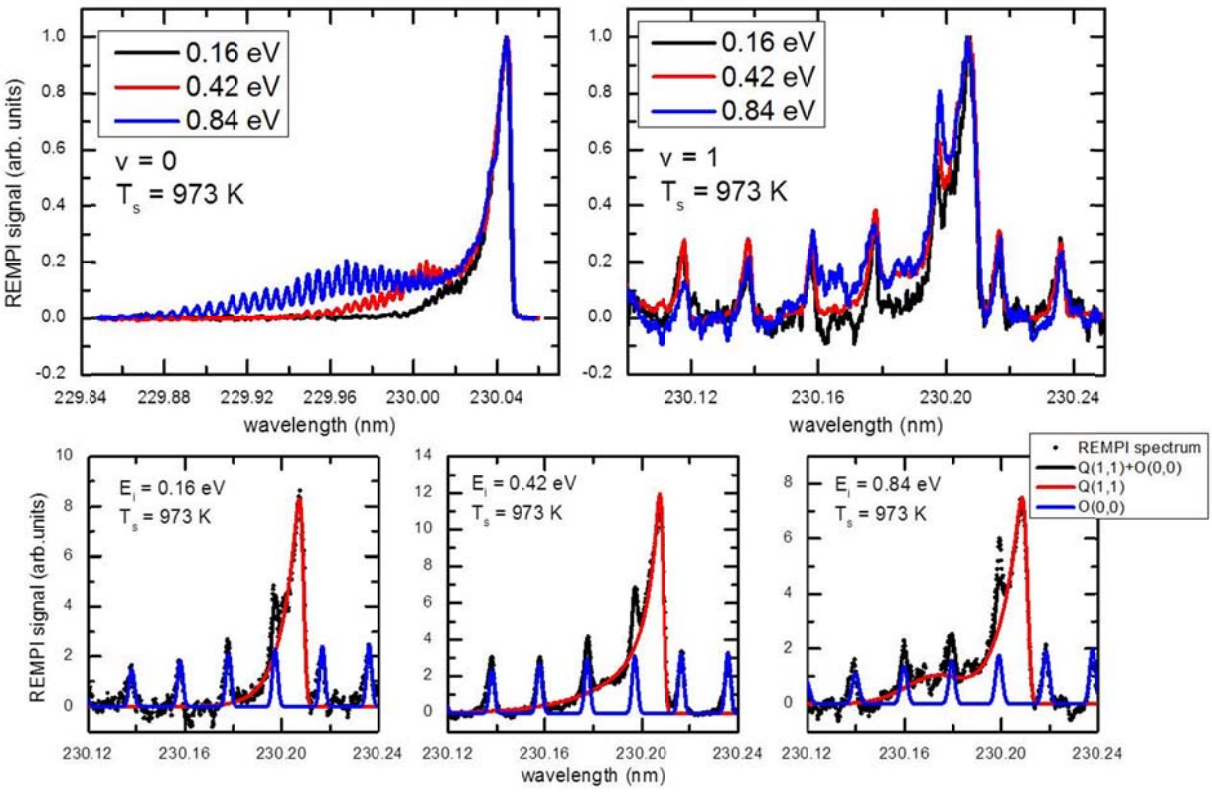

Figure 3: (Upper row) REMPI spectra of the scattered CO molecules in the $v = 0$ (left) and $v = 1$ state (right) measured at T_s = 973 K for three different E_i (0.16, 0.42 and 0.84 eV). For molecules scattered in both $v = 0$ and 1 states, the rotational distribution is non-thermal and is strongly influenced by the E_i. The spectra are peak normalized for the sake of comparison. Shown in the lower panel are examples of the fit to the REMPI spectra (T_s = 973 K, E_i = 0.16, 0.42 and 0.84 eV) in the Q(1,1) band region using a fit function as a sum of the individual Q(1,1) and O(0,0) components. The individual Q(1,1) and O(0,0) components are also shown.

The angular distributions were measured both as a function of E_i and T_s and some of these results are shown in Fig 4. The CO angular distributions for both v = 0 and 1 were narrower than a cosine function – shown as red dashed curve in Fig. 4 – indicating that a majority of the molecules undergo direct inelastic scattering. It can also be seen that the angular distributions for the scattered CO molecules in the $v = 1$ state are broader than those for $v = 0$. Moreover, the angular distributions for $v = 1$ become broader with increasing T_s whereas those for $v = 0$ do not change significantly. In order to correct for these effects in the evaluation of vibrational excitation probabilities, the angular distributions were fit to a peak normalized Gaussian function with the following form:

$$f(\theta) = Exp[-\frac{(\theta - \theta_0)^2}{2\sigma^2}]$$

The parameter σ (see Table 2) is a measure of the width of the distribution and θ_0 represents the specular reflection angle.

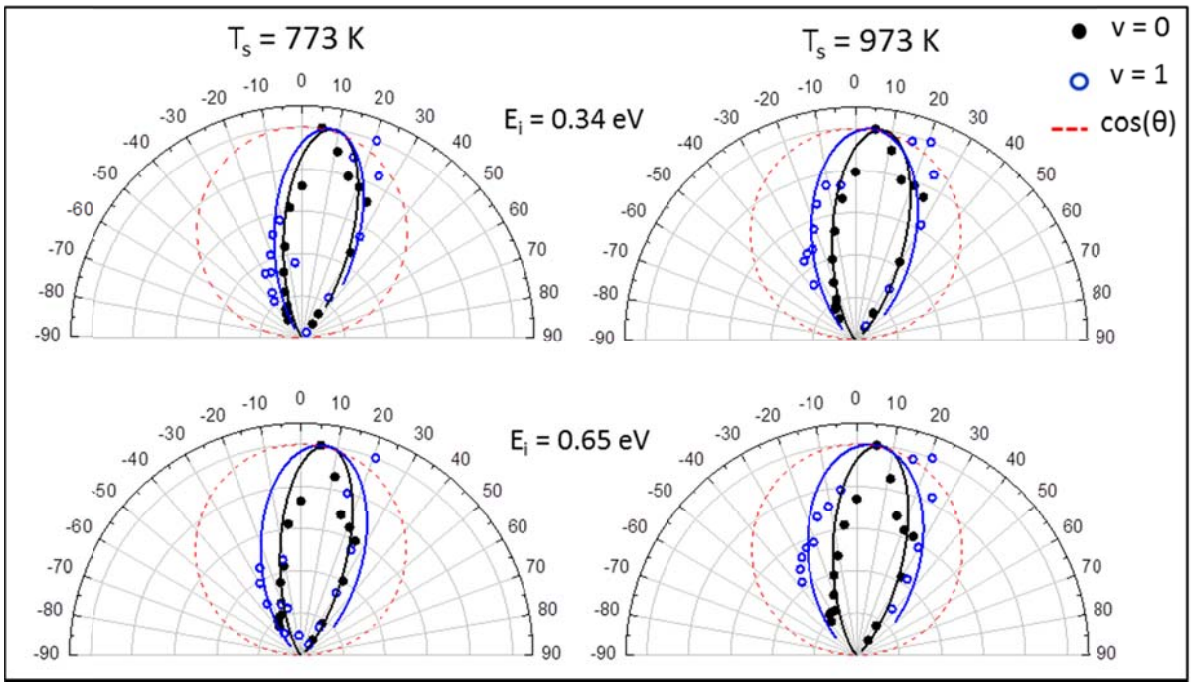

Figure 4: Angular distributions observed for the scattered $v = 0$ (filled circles) and 1 (open circles) molecules measured at 773 and 973 K for two different E_i. For a given T_s the distributions for $v = 1$ are broader than those for the $v = 1$ and their width increases with T_s. The lines are the fits to the data using a Gaussian function as described in text. For the$v = 1$, due to significant background contribution the points between 0 and 10° are excluded. Note that the distributions observed are much narrower than the cosine distribution (red dashed curve) indicating that the direct inelastic scattering is the dominant channel.

At E_i = 0.16 and 0.84 eV, due to experimental limitations, the angular distributions for the molecules in $v = 1$ could not be measured accurately. In the absence of these values we make some approximations in order to account for the correction arising due to spatial dilution. At E_i = 0.84 eV the correction factor for the angular distribution is assumed to be identical to that for E_i = 0.65 eV. This is reasonable because in this small range of E_i (0.65 to 0.84 eV), the scattering dynamics are expected to remain unchanged resulting in similar angular distributions. At E_i = 0.16 eV this correction factor is expected to be the biggest as trapping/desorption is the dominant channel for the vibrational excitation (this is discussed in more detail below). At this incidence energy, if all the $v = 1$ molecules arise from trapping/desorption and if the sticking probability were unity, the angular distribution is expected to follow a cosine distribution. In this case the correction factor due to the angular distribution is about 2 – we take this as an upper limit to the correction. The temporal profiles for the scattered molecules in v = 0 and 1 were measured individually at different T_s for each E_i and the correction for the temporal dilution was calculated in a similar manner.

Since the REMPI signal is proportional to number density, detection sensitivity depends on the velocity at which the molecules move through the probe volume. However, due to insufficient signal-to-noise ratio, the speed distribution of the scattered molecules in $v = 1$ could not be measured using

the time-of-flight methods that were employed in similar experiments with NO/Au(111).[7] Nonetheless, recently reported measurements on the NO/Au(111) system [21] show that in systems exhibiting EHP-V transfer, vibration is weakly coupled to translation. Based on this it is reasonable to assume that the velocity distributions for the scattered molecules in the $v = 0$ and 1 states are similar, resulting in only a small correction, which we neglect.

Table 2: The parameters obtained from the angular distribution measurements at different T_s and E_i values. The angular distributions were fit to a normalized Gaussian function. The parameter σ is a measure of the width of the distribution and θ_0 is the peak of the angular distribution. For E_i = 0.16 and 0.84 eV, the angular distributions for $v = 1$ could not be measured accurately due to experimental limitations. The uncertainties on σ and θ_0 are ± 1° and ± 2° for the $v = 0$, and 1, respectively.

E_i (eV)	T_s (K)	$v = 0$		$v = 1$	
		σ(deg)	θ_0(deg)	σ(deg)	θ_0(deg)
0.16	573	17	8	na	na
	773	17	5	na	na
	973	19	4	na	na
0.34	573	17	9	12	10
	773	16	9	19	8
	973	17	7	24	4
0.42	573	16	8	18	11
	773	16	7	20	8
	973	16	6	24	5
0.5	573	16	9	16	13
	773	16	8	22	6
	973	17	7	26	4
0.65	573	15	8	13	11
	773	16	7	24	6
	973	16	6	27	4
0.84	573	15	7	na	na
	773	15	6	na	na
	973	14	6	na	na

The absolute vibrational excitation probabilities obtained as a function of T_s measured at six different translational incidence energies are shown in Fig. 5. For a given translational incidence energy, the vibrational excitation probabilities increase with increasing T_s. Also shown (red dashed line) are the fits to the observed data with an Arrhenius equation:

$$P(v = 0 \rightarrow 1) = \ A(E_i) \times \exp(-\frac{\Delta E_{vib}}{kT})$$

Where ΔE_{vib} is the CO $v = 0 \rightarrow 1$ vibrational energy gap (2143 cm^{-1}), k is the Boltzmann constant, T is the temperature in Kelvin and $A(E_i)$ is the incidence translational energy dependent pre-factor, which may vary between 0 and 1. Note that $A(E_i) = 1$ corresponds to thermal equilibrium. Figure 6 shows the results of Fig. 5 as an Arrhenius plot. All vibrational excitation probabilities are one-tenth of the thermal limit – shown as a dashed line – or less, except at the lowest incidence energies and surface temperatures.

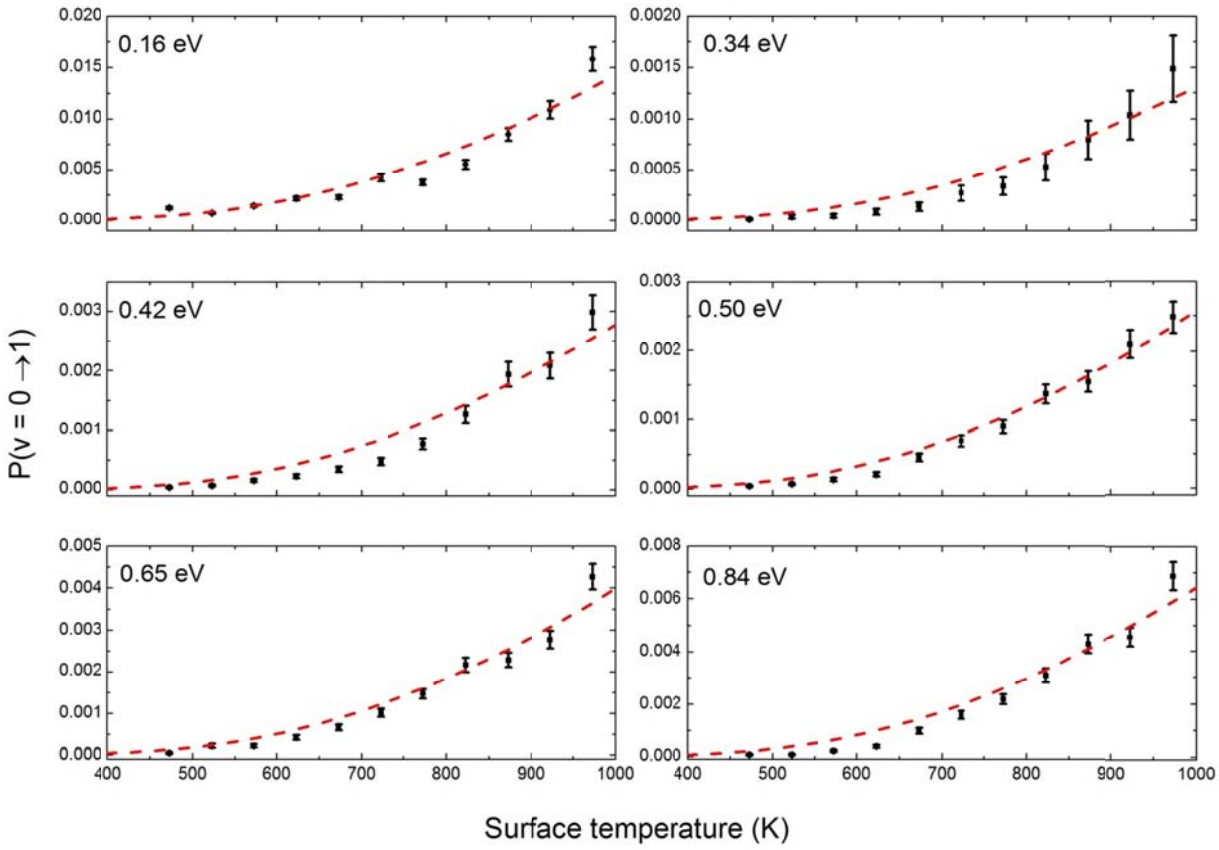

Figure 5: Absolute vibrational excitation probabilities ($v = 0 \rightarrow 1$) as a function of surface temperature measured at different E_i. Note that the Y scale is different in each of the plots. The dashed curve (red) represents the fit using the Arrhenius equation (see text).

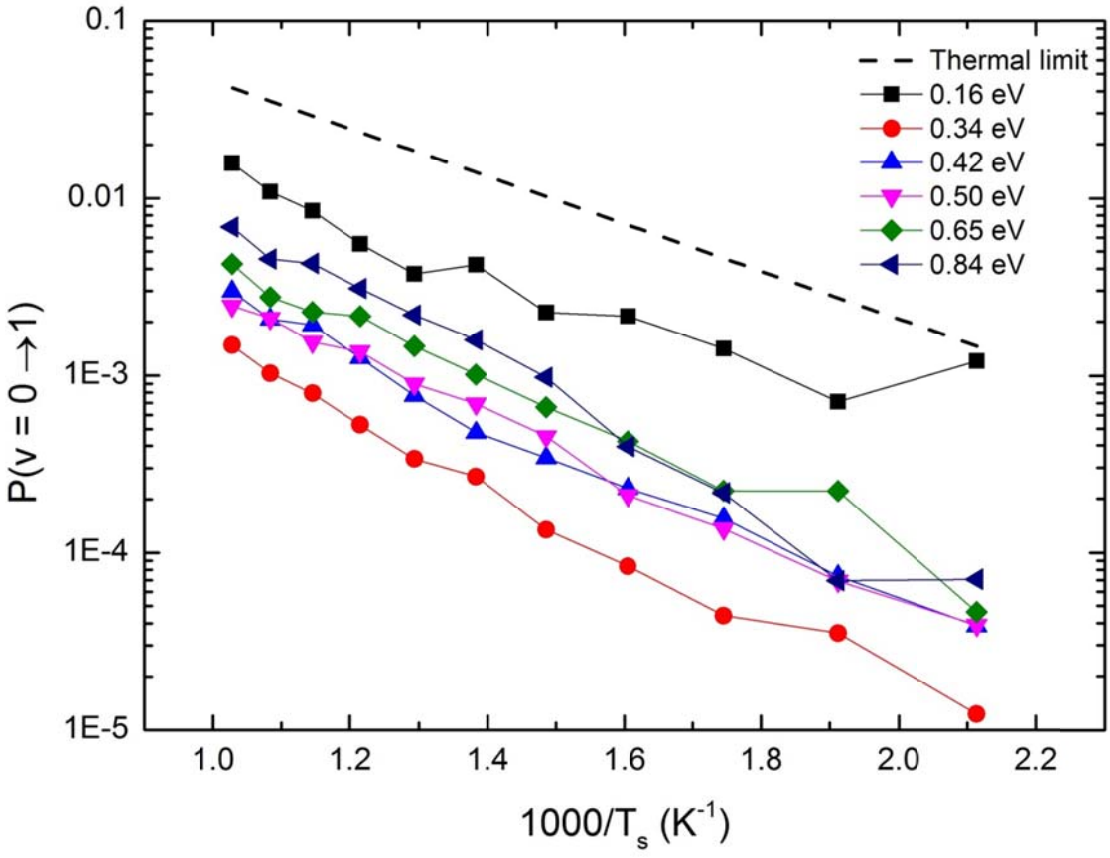

Figure 6: Arrhenius plot for the observed vibrational excitation probabilities at different T_s measured at different incidence energies. The dashed curve depicts the fraction of $v = 1$ molecules as expected from thermal equilibrium (thermal limit). The error bars have been omitted in this plot for the sake of clarity.

The E_i dependence of the vibrational excitation probabilities is shown in Fig 7. These values are plotted for different values of T_s. Both above and below 0.34 eV, the vibrational excitation probabilities increase. This is an indication that the dynamics of scattering changes at low incidence energy. For the sake of comparison, the trapping probabilities (at 100 K) reported by Rettner are also shown in Fig. 7 (inset). This curve shows that the trapping probability is significantly large at low E_i – hence, we expect that at E_i = 0.16 eV the vibrational excitation has a significant contribution from trapping/desorption.

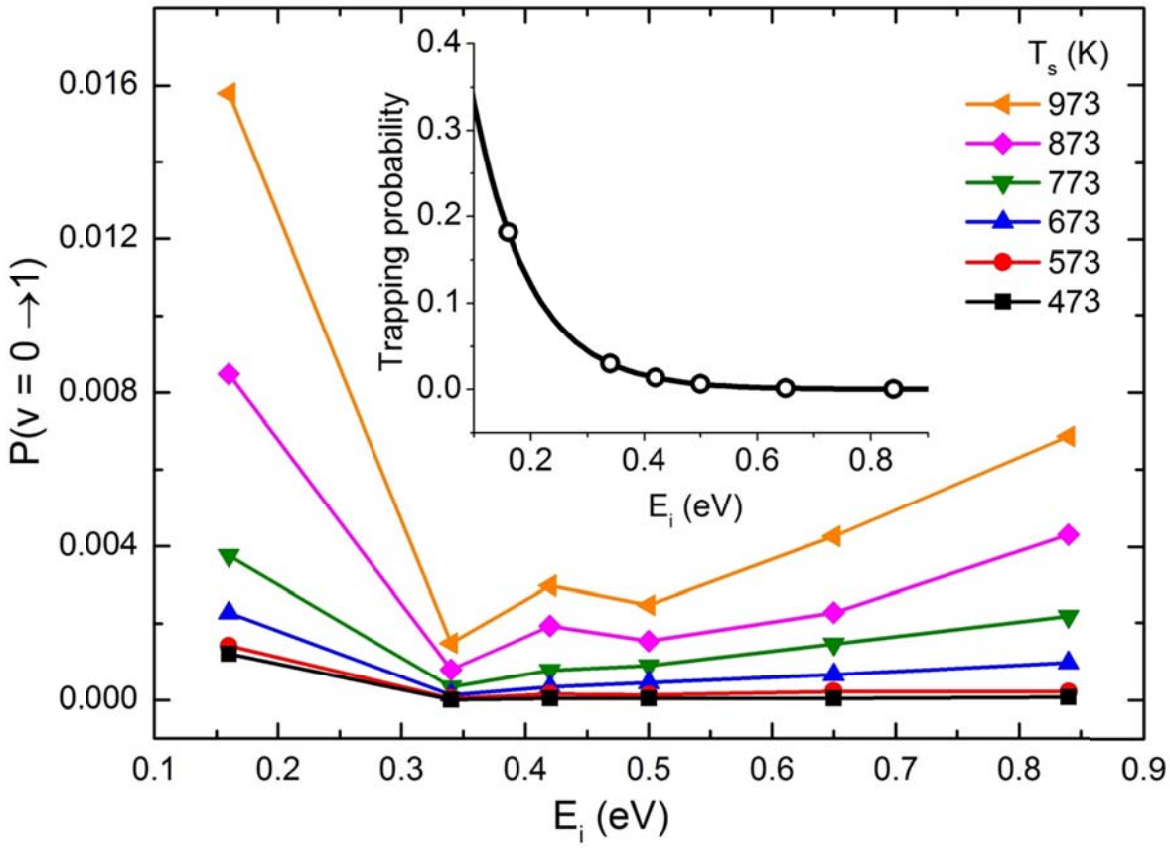

Figure 7: The vibrational excitation probabilities as a function of the E_i for a given T_s. Clearly, the vibrational excitation probabilities first decrease and then increase with the E_i. The error bars have been omitted for the sake of clarity. Also shown in the inset is the trapping probability of CO on Au(111) at a surface temperature of 100 K reported by Rettner [16]. The open circles denote the E_i at which the present measurements were carried out.

The pre-factors obtained from the Arrhenius fits are plotted versus E_i in Fig.8. Also shown here are the pre-factors reported for the NO/Au(111) system.[7] The pre-factors for CO/Au(111) are smaller by only about a factor of 2-3 (except at E_i = 0.16 eV which is influenced by trapping/desorption) as compared to NO/Au(111) indicating that the magnitude of the non-adiabatic coupling strength in case of CO is only somewhat weaker than that for NO.

The vibrational excitation observed via the trapping desorption channel raises an important question: Do the "trapped" molecules completely thermalize their vibration before they desorb or not? In order to answer this question, one needs to compare the residence time of the CO molecules trapped on the surface with the timescale for the vibrations to come to equilibrium with the surface.

Temperature programmed desorption measurements show that the binding energy of CO on Au(111) is approximately 0.14 eV and the Arrhenius prefactor to be of the order of 10^{13} Hz.[22] Based on these values, the estimated residence time (inverse of the desorption rate constant, obtained using Arrhenius

equation for desorption) of CO molecules trapped on the Au(111) surface ranges from 10^{-11} to 10^{-13} sec in the temperature range of 300 to 1000 K.

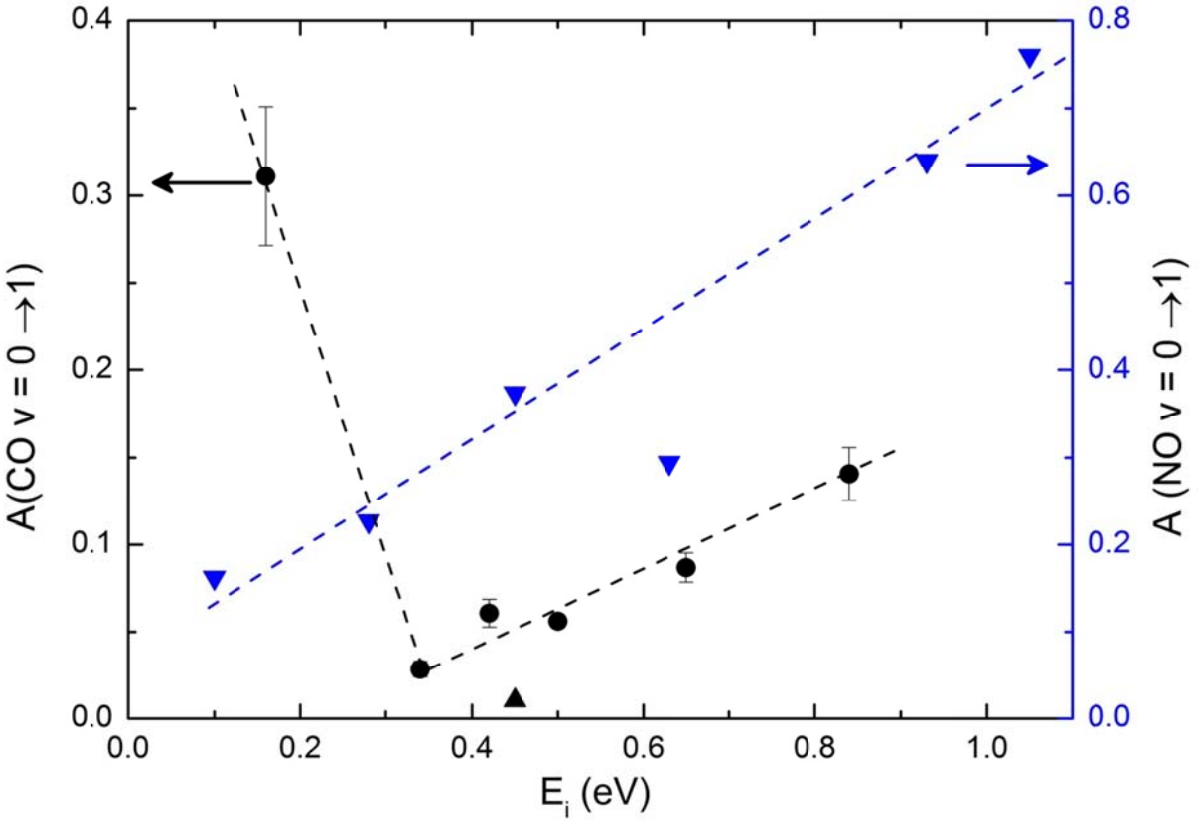

Figure 8: Pre-factors obtained from the Arrhenius fit at different incidence energies (black dots) for CO. The downward pointing triangles (blue) are the pre-factors previously reported for NO vibrational excitation ($v = 0 \rightarrow 1$) upon scattering from Au(111).[7] The pre-factors for CO first decrease and then increase with E_i in contrast to those for NO, which increase monotonically with E_i. The upward pointing triangle denotes the previously reported value.[15] The dashed lines are shown purely as a guide to the eye to highlight the observed trends. The arrows denote the Y axis corresponding to the data (left: CO and right: NO)

The vibration relaxation rate of the adsorbed molecules is a measure of the timescale required for the vibrational degree of freedom of the trapped molecules to come to thermal equilibrium with the surface. Previous work shows that the vibrational relaxation timescales of CO adsorbed on metal surfaces such as Pt and Cu is of the order of a few picoseconds.[1, 23] If one assumes that the vibration relaxation times are similar in the present case, then at higher temperatures (shorter residence times) there could be a situation that the molecules desorb before the vibrational degree of freedom is in equilibrium with the surface. Such an effect indeed has been reported for NO desorbing from Pt(111).[24] However, to the best of our knowledge the vibrational relaxation time for CO adsorbed on Au(111) is not known. More importantly, whether vibrational relaxation timescales are of the order of picoseconds for all metal molecule systems, irrespective of the strength of the interaction (physisorption vs. chemisorption) is an open question still. In absence of this information, it is

difficult to say if in the present case the CO molecules have vibrationally equilibrated before desorption or not.

An additional remark we make here is regarding the mechanism of vibration excitation in the trapping desorption channel. We believe that in this case too (similar to the direct scattering) the vibration excitation occurs predominantly via the EHP-V mechanism simply because it is much more probable than energy transfer via phonons which involve multi-phonon transitions. A quantitative comparison of the rates of EHP-V vs phonon-adsorbate energy transfer again requires the knowledge of the vibration relaxation timescales which is presently unavailable. Some aspects of this question are currently being pursued in our lab by looking at the relaxation of vibrationally excited CO molecules on a clean Au(111) surface, and hopefully these measurements will be able to shed more light on this issue in the near future.

In summary, in this work we have carried out comprehensive measurements of the $v = 0 \rightarrow 1$ vibrational excitation probabilities for CO scattering from Au(111) as a function of the translational incidence energy and surface temperature. Our measurements show that the angular distributions of the scattered molecules are narrow and that for a given $E_{i,}$ the vibrational excitation probabilities are strongly dependent on T_s. These observations are consistent with EHP-V energy transfer occurring via a single bounce, direct scattering event. The vibrational excitation probability at a fixed surface temperature was also found to increase with increasing E_i. However, at the lowest E_i (0.16 eV) the vibrational excitation probability and Arrhenius pre-factor (A) values were observed to be exceptionally high. We attribute this increase to be caused by the increased contribution of trapping/desorption at low E_i.

ACKNOWLEDGMENTS

A.M.W would like to acknowledge the support from Alexander von Humboldt Foundation

Appendix:

Table 3: The absolute vibrational excitation probabilities P($v = 0 \rightarrow 1$) and their uncertainties (ΔP) as a function of surface temperature measured at different translational incidence energies.

	E_i = 0.16 eV		E_i = 0.34 eV		E_i = 0.42 eV	
T_s (K)	P($v = 0 \rightarrow 1$)	ΔP	P($v = 0 \rightarrow 1$)	ΔP	P($v = 0 \rightarrow 1$)	ΔP
473	1.2×10^{-3}	1×10^{-4}	1.2×10^{-5}	7×10^{-6}	3.9×10^{-5}	7×10^{-6}
523	7.1×10^{-4}	7×10^{-5}	3×10^{-5}	2×10^{-5}	7×10^{-5}	1×10^{-5}
573	1.4×10^{-3}	1×10^{-4}	4×10^{-5}	2×10^{-5}	1.6×10^{-4}	2×10^{-5}
623	2.2×10^{-3}	2×10^{-4}	8.4×10^{-5}	3×10^{-5}	2.3×10^{-4}	3×10^{-5}
673	2.3×10^{-3}	2×10^{-4}	1.3×10^{-4}	4×10^{-5}	3.4×10^{-4}	5×10^{-5}
723	4.2×10^{-3}	3×10^{-4}	2.7×10^{-4}	8×10^{-5}	4.8×10^{-4}	6×10^{-5}
773	3.8×10^{-3}	3×10^{-4}	3.4×10^{-4}	9×10^{-5}	7.7×10^{-4}	9×10^{-5}
823	5.5×10^{-3}	4×10^{-4}	5.3×10^{-4}	1×10^{-4}	1.3×10^{-3}	1×10^{-4}
873	8.5×10^{-3}	6×10^{-4}	7.9×10^{-4}	2×10^{-4}	1.9×10^{-3}	2×10^{-4}
923	1.1×10^{-2}	9×10^{-4}	1.0×10^{-3}	2×10^{-4}	2.1×10^{-3}	2×10^{-4}
973	1.6×10^{-2}	1×10^{-3}	1.5×10^{-3}	3×10^{-4}	3.0×10^{-3}	3×10^{-4}

	E_i = 0.50 eV		E_i = 0.65 eV		E_i = 0.84 eV	
T_s (K)	P($v = 0 \rightarrow 1$)	ΔP	P($v = 0 \rightarrow 1$)	ΔP	P($v = 0 \rightarrow 1$)	ΔP
473	4×10^{-5}	1×10^{-5}	5×10^{-5}	1×10^{-5}	7×10^{-5}	2×10^{-5}
523	7×10^{-5}	1×10^{-5}	2.2×10^{-4}	5×10^{-5}	7×10^{-5}	2×10^{-5}
573	1.4×10^{-4}	2×10^{-5}	2.2×10^{-4}	4×10^{-5}	2.2×10^{-4}	4×10^{-5}
623	2.1×10^{-4}	3×10^{-5}	4.2×10^{-4}	6×10^{-5}	4.0×10^{-4}	6×10^{-5}
673	4.5×10^{-4}	6×10^{-5}	6.6×10^{-4}	7×10^{-5}	10×10^{-4}	1×10^{-4}
723	6.9×10^{-4}	8×10^{-5}	1.0×10^{-3}	9×10^{-5}	1.6×10^{-3}	2×10^{-4}
773	9.0×10^{-4}	9×10^{-5}	1.5×10^{-3}	1×10^{-4}	2.2×10^{-3}	2×10^{-4}
823	1.4×10^{-3}	1×10^{-4}	2.2×10^{-3}	2×10^{-4}	3.1×10^{-3}	3×10^{-4}
873	1.5×10^{-3}	1×10^{-4}	2.3×10^{-3}	2×10^{-4}	4.3×10^{-3}	4×10^{-4}
923	2.1×10^{-3}	2×10^{-4}	2.8×10^{-3}	2×10^{-4}	4.5×10^{-3}	4×10^{-4}
973	2.5×10^{-3}	2×10^{-4}	4.3×10^{-3}	3×10^{-4}	6.9×10^{-3}	5×10^{-4}

References

1. H. Arnolds, Prog Surf Sci 86 (1-2), 1 (2011).
2. J. C. Tully, Annu Rev Phys Chem 51, 153 (2000).
3. A. M. Wodtke, D. Matsiev and D. J. Auerbach, Prog Surf Sci 83 (3), 167 (2008).
4. B. D. Kay, T. D. Raymond and M. E. Coltrin, Phys Rev Lett 59 (24), 2792 (1987).
5. C. T. Rettner, F. Fabre, J. Kimman and D. J. Auerbach, Phys Rev Lett 55 (18), 1904 (1985).
6. R. Cooper, C. Bartels, A. Kandratsenka, I. Rahinov, N. Shenvi, K. Golibrzuch, Z. S. Li, D. J. Auerbach, J. C. Tully and A. M. Wodtke, Angew Chem Int Edit 51 (20), 4954 (2012).
7. R. Cooper, Z. S. Li, K. Golibrzuch, C. Bartels, I. Rahinov, D. J. Auerbach and A. M. Wodtke, Journal of Chemical Physics 137 (6), 064705 (2012).
8. M. Born and R. Oppenheimer, Ann Phys-Berlin 84 (20), 0457 (1927).
9. Y. H. Huang, C. T. Rettner, D. J. Auerbach and A. M. Wodtke, Science 290 (5489), 111 (2000).
10. J. D. White, J. Chen, D. Matsiev, D. J. Auerbach and A. M. Wodtke, Nature 433 (7025), 503 (2005).
11. M. Head-Gordon and J. C. Tully, J Chem Phys 103 (23), 10137 (1995).
12. N. Shenvi, S. Roy and J. C. Tully, Science 326 (5954), 829 (2009).
13. N. Shenvi, S. Roy and J. C. Tully, J Chem Phys 130 (17), 174107 (2009).
14. S. Monturet and P. Saalfrank, Phys Rev B 82 (7), 075404 (2010).
15. T. Schäfer, N. Bartels, K. Golibrzuch, C. Bartels, H. Kockert, D. J. Auerbach, T. N. Kitsopoulos and A. M. Wodtke, Phys Chem Chem Phys 15 (6), 1863 (2013).
16. C. T. Rettner, J Chem Phys 99 (7), 5481 (1993).
17. Q. Ran, D. Matsiev, A. M. Wodtke and D. J. Auerbach, Rev Sci Instrum 78 (10) (2007).
18. M. A. Hines and R. N. Zare, J Chem Phys 98 (11), 9134 (1993).
19. A. W. Kleyn and T. C. M. Horn, Phys Rep 199 (4), 192 (1991).
20. See Supplementary Material Document No._____ for additional fits and best fit parameters.
21. K. Golibrzuch, P. R. Shirhatti, J. Altschaffel, I. Rahinov, D. J. Auerbach, A. M. Wodtke and C. Bartels, J Phys Chem A 117 (36), 8750 (2013).
22. E. Dan. (personal communication)
23. H. Ueba, Prog Surf Sci 55 (2), 115 (1997).
24. M. Asscher, G. A. Somorjai and Y. Zeiri, J Chem Phys 81 (3), 1507 (1984).

Supplementary information

Evidence for two vibrational excitation channels in collisions of CO with a Au(111) surface

Authors: Pranav R. Shirhatti, Jörn Werdecker, Kai Golibrzuch, Alec M. Wodtke, Christof Bartels

SI1: Examples of the fit to the REMPI spectra at different E_i and T_s.

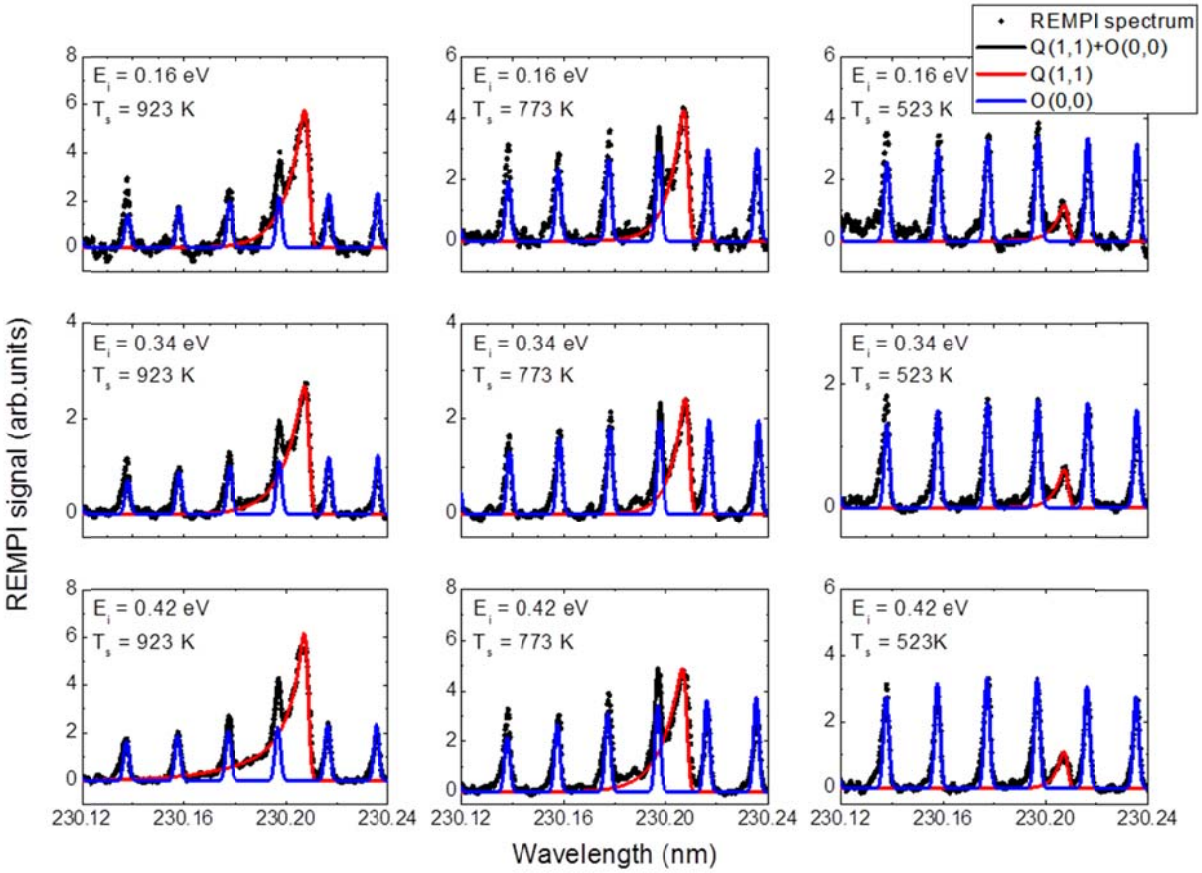

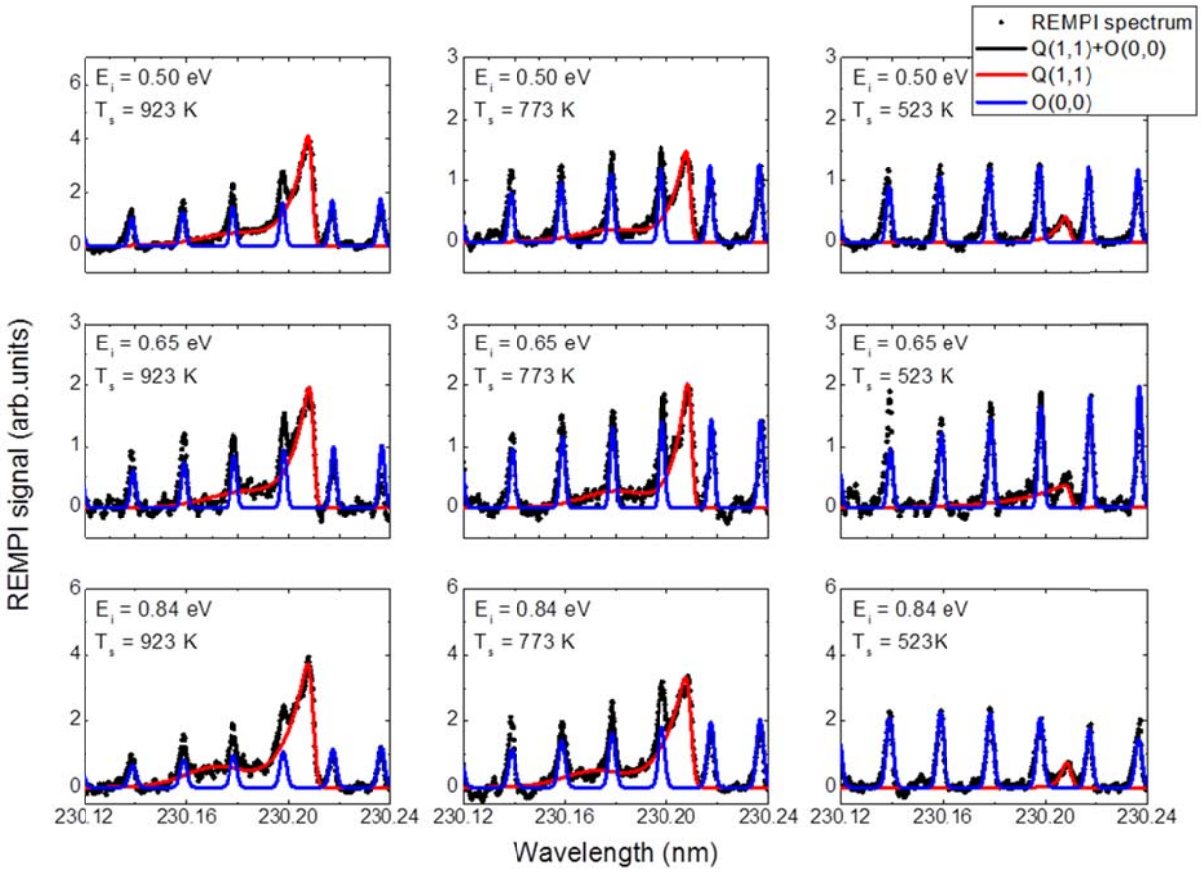
REMPI spectrum
Q(1,1)+O(0,0)
Q(1,1)
O(0,0)
E_i = 0.50 eV
T_s = 923 K
E_i = 0.50 eV
T_s = 773 K
E_i = 0.50 eV
T_s = 523 K
E_i = 0.65 eV
T_s = 923 K
E_i = 0.65 eV
T_s = 773 K
E_i = 0.65 eV
T_s = 523 K
E_i = 0.84 eV
T_s = 923 K
E_i = 0.84 eV
T_s = 773 K
E_i = 0.84 eV
T_s = 523K
REMPI signal (arb.units)
Wavelength (nm)
230.12
230.16
230.20
230.24

SI2: The parameters obtained from fitting the REMPI spectra of the scattered molecules in v = 0 and 1 state.

E_i = 0.16 eV; v = 0					v = 1			
T_s	T_{rot} (K)	a_r	a_0	a_1	T_{rot} (K)	a_r	a_0	a_1
473	287	1.6	20	4	1028	0	na	na
523	333	1.5	20	3	249	0	na	na
573	311	1.4	20	3	433	0	na	na
623	324	1.4	20	4	483	0	na	na
673	309	1.6	20	4	363	0	na	na
723	309	1.6	20	5	496	0	na	na
773	345	1.4	21	4	366	0	na	na
823	325	1.7	21	4	433	0	na	na
873	360	1.7	21	3	489	0	na	na
923	345	1.6	21	5	446	0	na	na
973	357	2.0	22	4	431	0	na	na

E_i = 0.34 eV; v = 0					v = 1			
T_s	T_{rot} (K)	a_r	a_0	a_1	T_{rot} (K)	a_r	a_0	a_1
473	270	3.2	22	6	129	0	na	na
523	274	3.3	22	6	230	0	na	na
573	298	3.2	23	5	199	0	na	na
623	267	3.1	22	7	275	0	na	na
673	341	3.6	23	5	296	0	na	na
723	296	3.1	23	6	490	0	na	na
773	319	3.4	23	6	338	0	na	na
823	370	3.5	24	5	503	0	na	na
873	341	3.9	23	6	468	0	na	na
923	318	3.4	23	6	497	0	na	na
973	358	3.5	24	6	524	0	na	na

E_i = 0.42 eV; v = 0					v = 1			
T_s	T_{rot} (K)	a_r	a_0	a_1	T_{rot} (K)	a_r	a_0	a_1
473	258	3.6	23	8	122	0	na	na
523	317	4.5	24	7	186	0	na	na
573	311	4.2	24	7	415	0	na	na
623	330	4.3	24	6	378	0	na	na
673	325	4.3	24	7	421	0	na	na
723	353	3.9	25	6	403	0	na	na
773	311	3.8	24	7	494	0	na	na
823	400	4.5	25	6	334	7.7	15	17
873	311	4.1	24	8	315	8.2	15	17
923	379	4.0	25	7	342	7.9	15	17
973	371	4.7	25	7	310	8.9	15	17

E_i = 0.50 eV; v = 0					v = 1			
T_s	T_{rot} (K)	a_r	a_0	a_1	T_{rot} (K)	a_r	a_0	a_1
473	338	4.2	26	7	179	0	na	na
523	351	4.6	26	6	274	0	na	na
573	346	4.0	26	7	218	5.1	28	7
623	384	4.6	26	7	243	3.7	28	7
673	372	4.5	26	7	323	5.7	28	7
723	366	4.2	26	7	421	4.5	28	7
773	400	4.9	26	7	393	4.6	28	7
823	395	4.4	27	7	449	4.1	28	7
873	381	4.9	26	8	382	4.6	28	7
923	386	4.6	26	8	450	3.9	28	7
973	329	4.2	26	9	387	4.5	28	7

E_i = 0.65 eV; v = 0					v = 1			
T_s	T_{rot} (K)	a_r	a_0	a_1	T_{rot} (K)	a_r	a_0	a_1
473	304	4.4	28	10	169	0	na	na
523	273	4.2	27	11	1118	0	na	na
573	311	4.5	28	10	350	5.8	27	7
623	316	4.3	28	10	273	6.6	27	7
673	293	4.1	27	10	452	3.1	27	7
723	343	4.8	28	10	515	5.3	27	7
773	304	4.5	28	11	341	4.6	27	7
823	303	4.6	27	12	426	5.2	27	7
873	330	4.8	28	11	413	5.6	27	7
923	434	4.8	29	10	470	4.2	27	7
973	350	5.1	28	11	469	5.6	27	7

E_i = 0.84 eV; v = 0					v = 1			
T_s	T_{rot} (K)	a_r	a_0	a_1	T_{rot} (K)	a_r	a_0	a_1
473	397	6.0	32	11	276	0	na	na
523	440	6.4	33	11	133	0	na	na
573	368	5.2	32	12	300	0	na	na
623	417	5.7	33	12	492	0	na	na
673	388	5.2	32	12	515	6.0	30	6
723	445	6.3	33	12	469	5.4	30	6
773	483	6.5	34	12	543	5.5	30	6
823	478	6.0	34	11	561	4.6	30	6
873	326	5.3	31	14	499	6.7	30	6
923	518	6.8	34	11	536	6.2	30	6
973	336	5.7	31	15	545	5.0	30	6

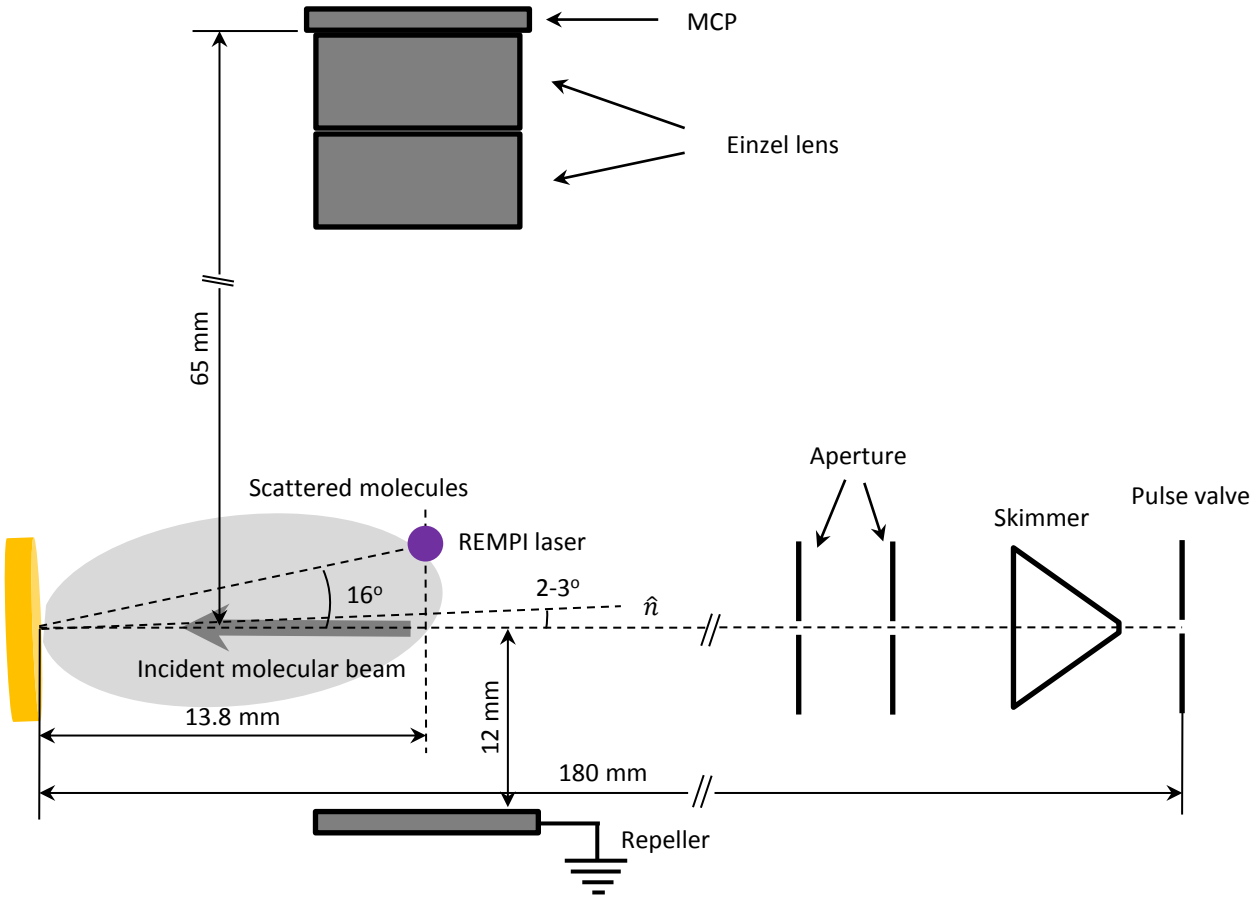
MCP
Einzel lens
65 mm
Scattered molecules
REMPI laser
16°
2-3°
$\hat{n}$
Incident molecular beam
13.8 mm
12 mm
180 mm
Repeller
Aperture
Skimmer
Pulse valve

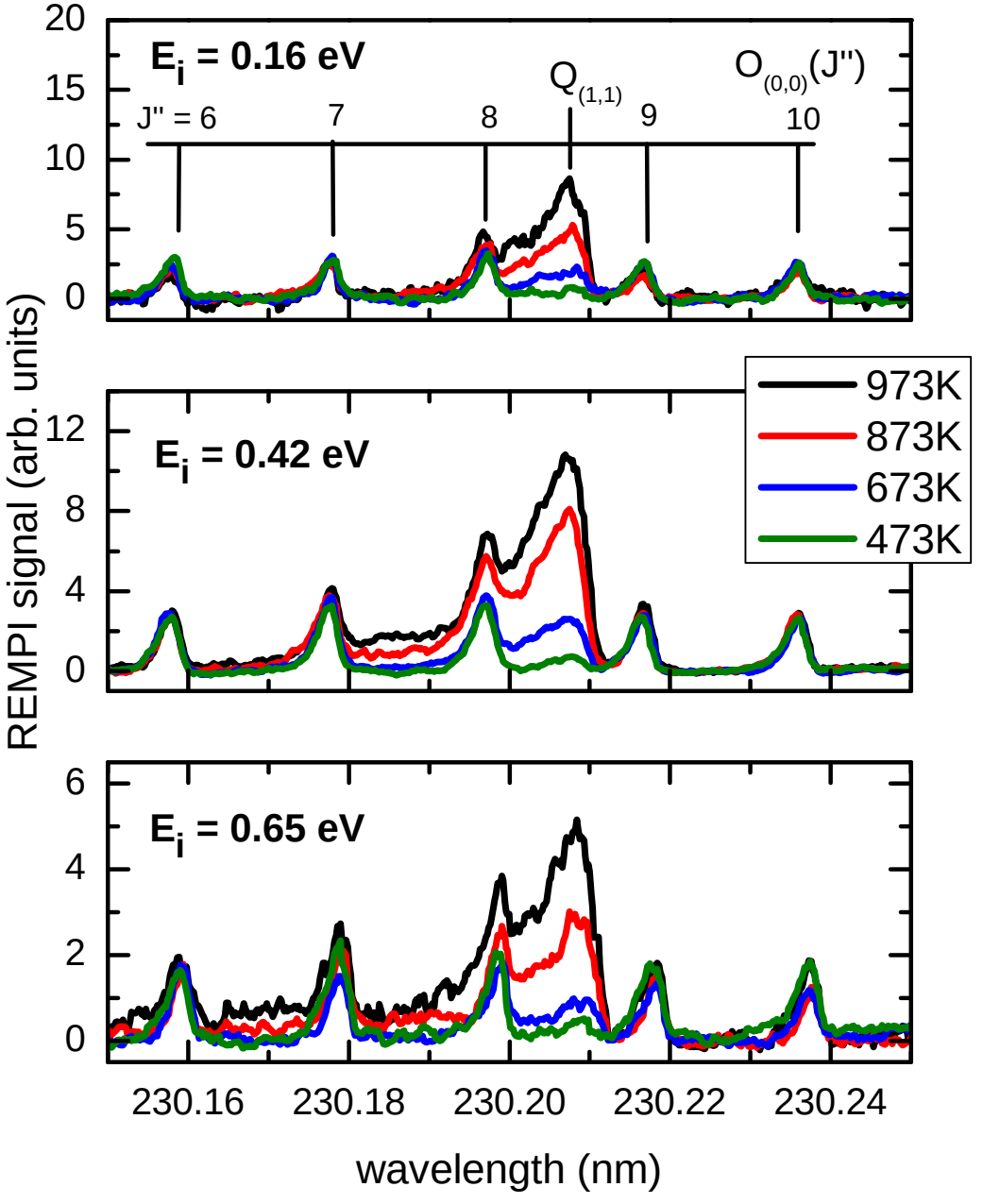
E_i = 0.16 eV
Q_(1,1)
O_(0,0)(J")
J" = 6
7
8
9
10
E_i = 0.42 eV
E_i = 0.65 eV
973K
873K
673K
473K
REMPI signal (arb. units)
wavelength (nm)
230.16
230.18
230.20
230.22
230.24

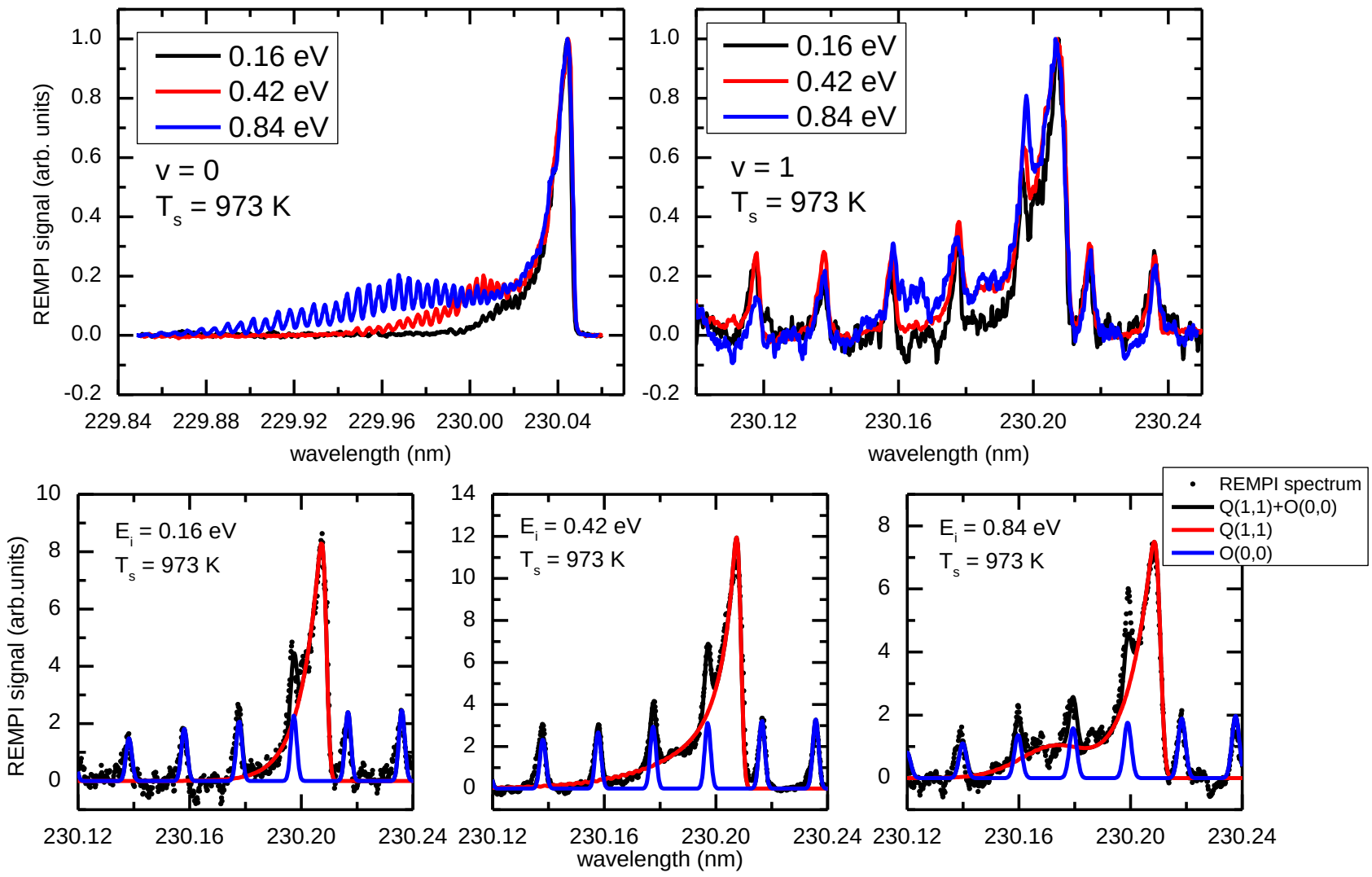
0.16 eV
0.42 eV
0.84 eV
v = 0
T_s = 973 K
REMPI signal (arb. units)
wavelength (nm)
v = 1
T_s = 973 K
E_i = 0.16 eV
E_i = 0.42 eV
E_i = 0.84 eV
REMPI signal (arb.units)
REMPI spectrum
Q(1,1)+O(0,0)
Q(1,1)
O(0,0)

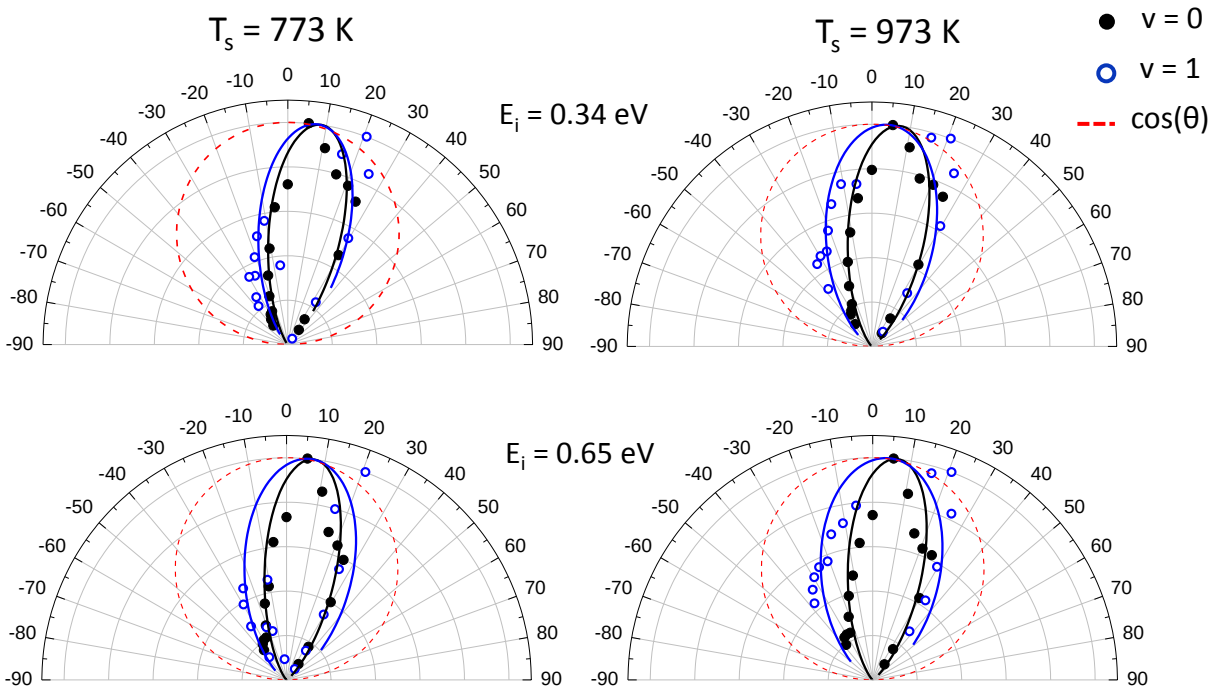
T_s = 773 K
T_s = 973 K
E_i = 0.34 eV
E_i = 0.65 eV
v = 0
v = 1
cos(θ)
-90
-80
-70
-60
-50
-40
-30
-20
-10
0
10
20
30
40
50
60
70
80
90

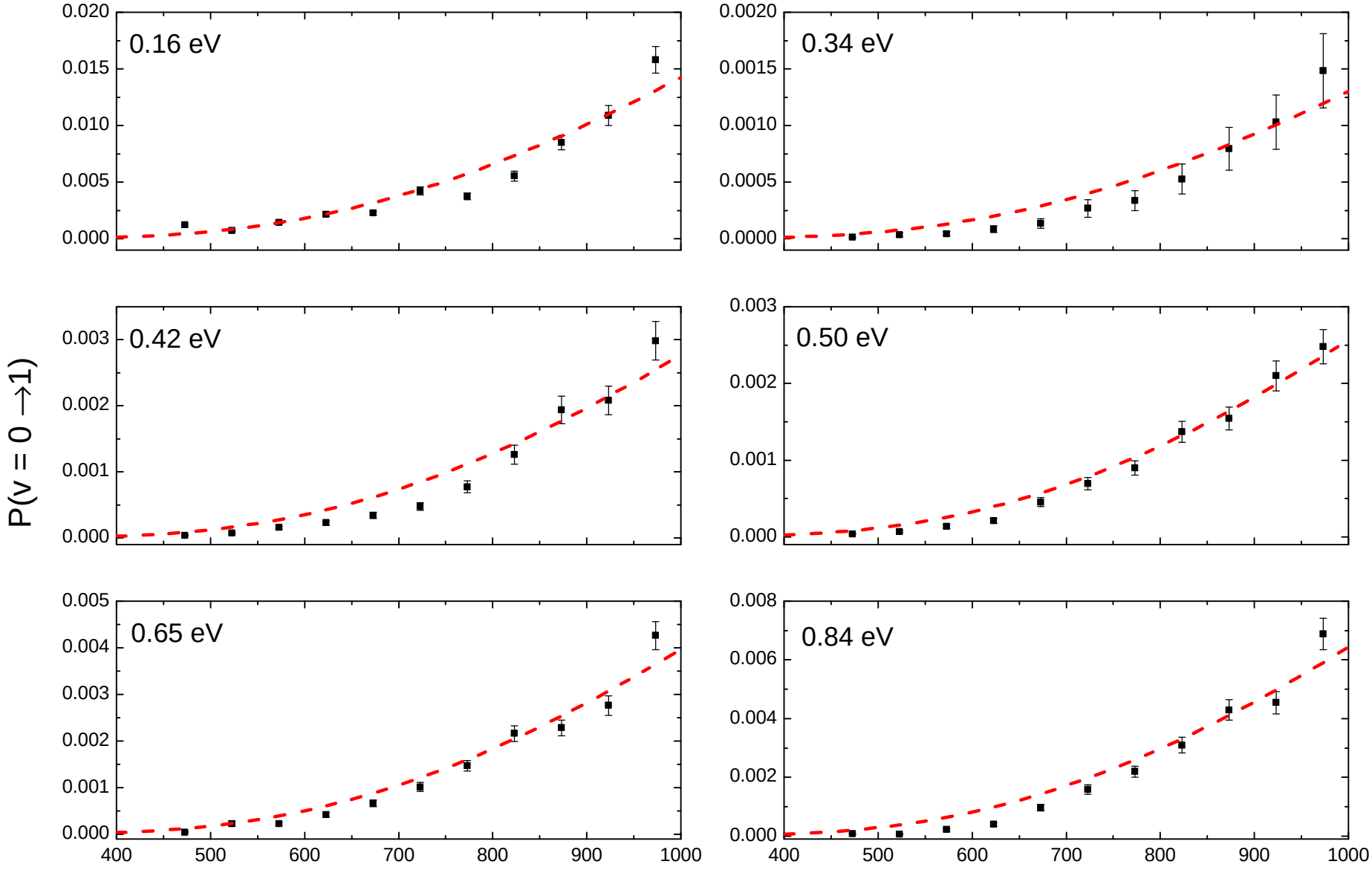
0.16 eV
0.34 eV
0.42 eV
0.50 eV
0.65 eV
0.84 eV
P(v = 0 →1)
Surface temperature (K)

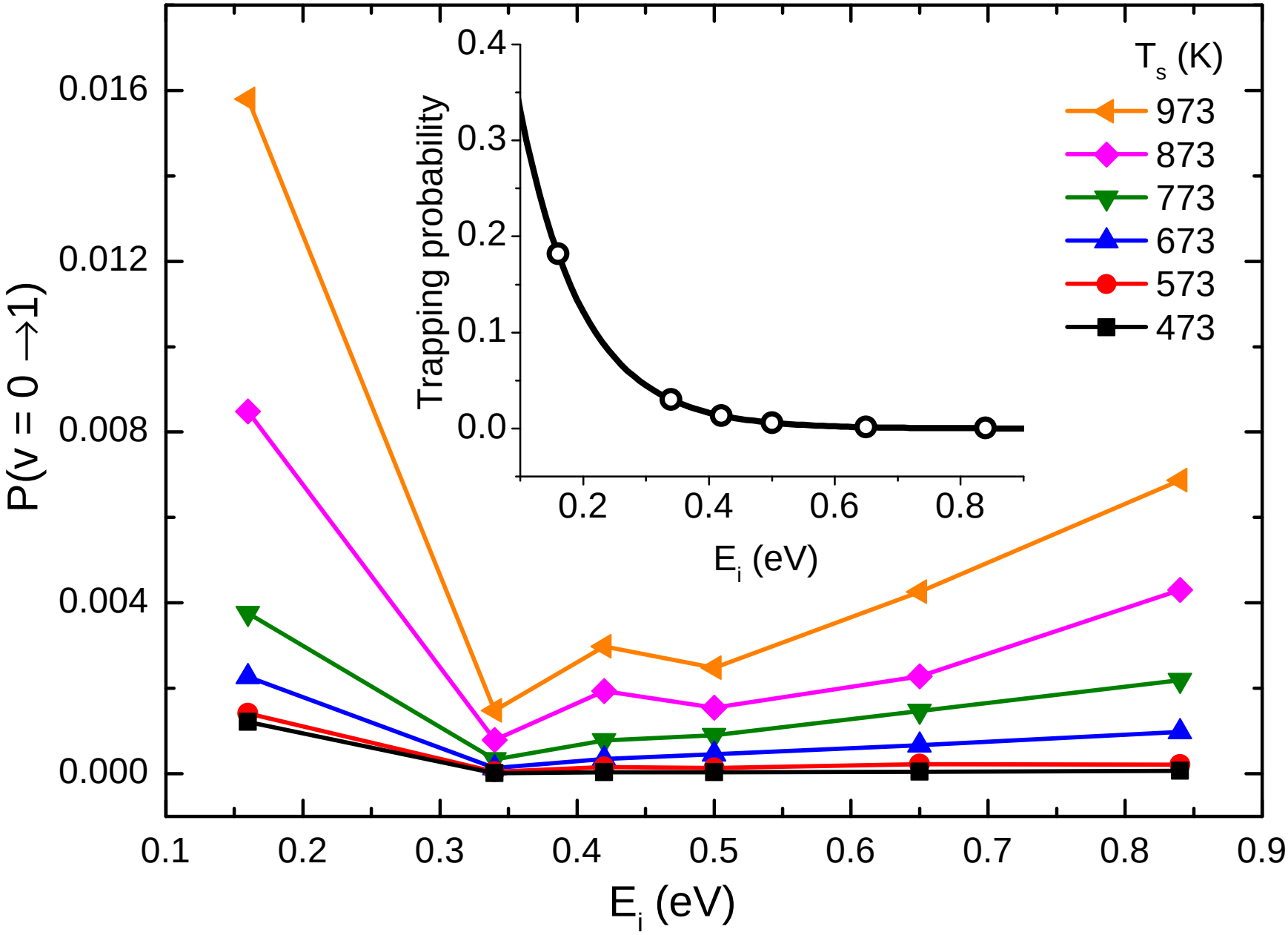
P(v = 0 →1)
0.016
0.012
0.008
0.004
0.000
0.1
0.2
0.3
0.4
0.5
0.6
0.7
0.8
0.9
E_i (eV)
T_s (K)
973
873
773
673
573
473
Trapping probability
0.4
0.3
0.2
0.1
0.0
0.2
0.4
0.6
0.8
E_i (eV)

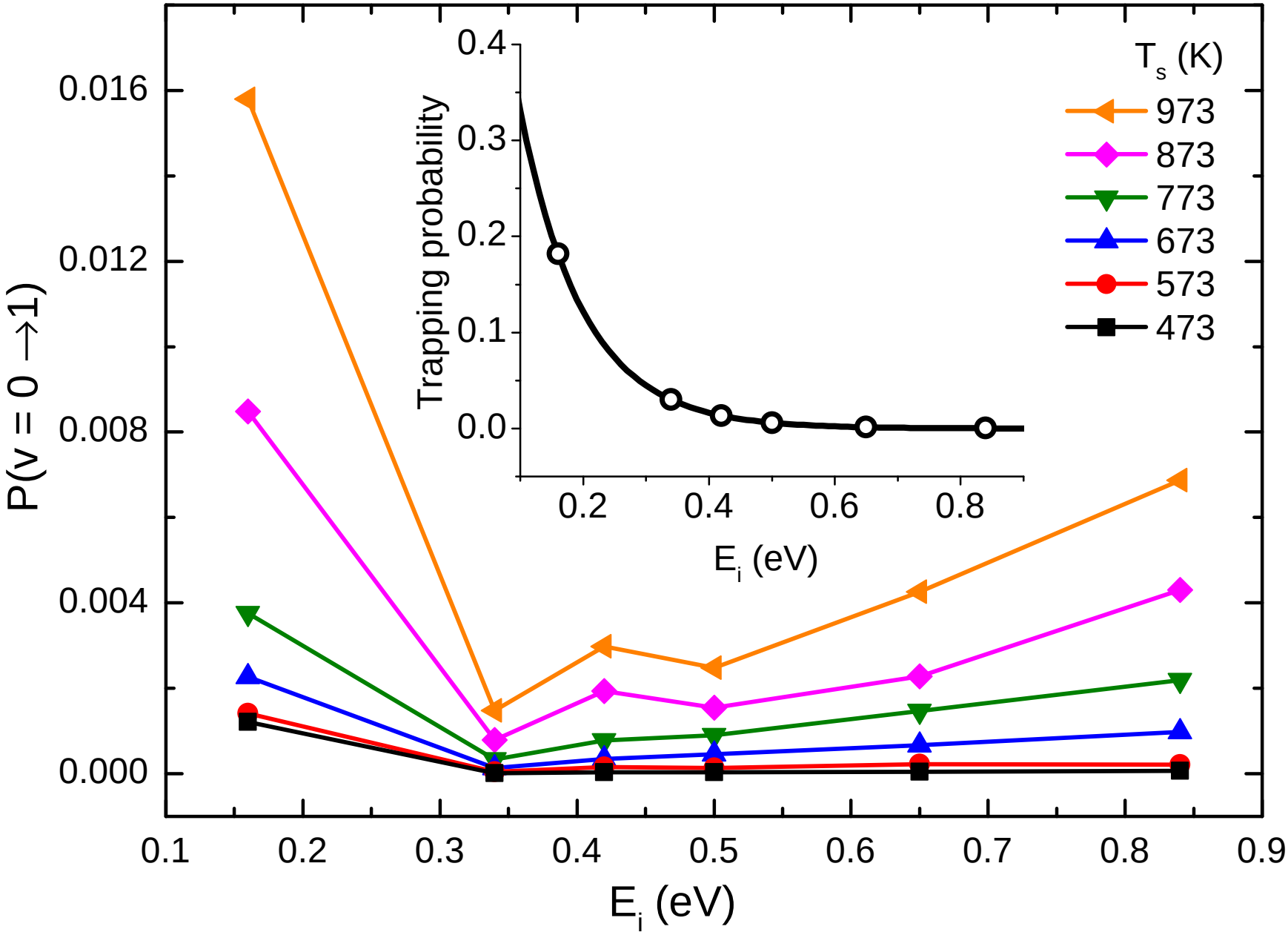
P(v = 0 →1)
0.016
0.012
0.008
0.004
0.000
0.1
0.2
0.3
0.4
0.5
0.6
0.7
0.8
0.9
E_i (eV)
T_s (K)
973
873
773
673
573
473
Trapping probability
0.4
0.3
0.2
0.1
0.0
0.2
0.4
0.6
0.8
E_i (eV)

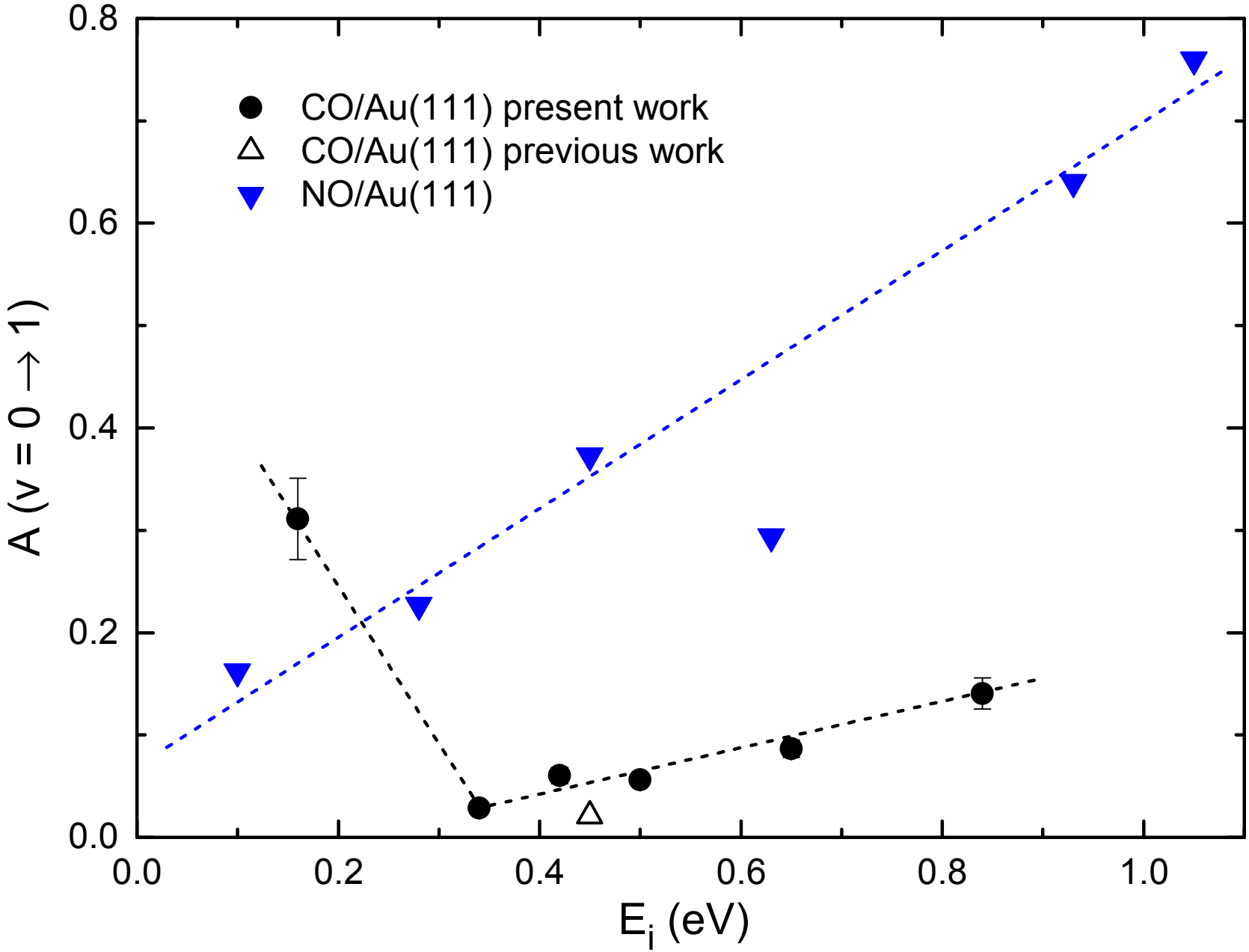
CO/Au(111) present work
CO/Au(111) previous work
NO/Au(111)
A (v = 0 → 1)
E_i (eV)
0.0
0.2
0.4
0.6
0.8
1.0